THE LIGHT HARVESTING PROCESS IN PURPLE BACTERIA*

B.P. Krueger, G.D. Scholes, J.-Y. Yu† and G.R. Fleming

Department of Chemistry, University of California at Berkeley and Physical Biosciences Division, Lawrence Berkeley National Laboratory, Berkeley, CA 94720-1460 U.S.A.

We present and review the results of fluorescence upconversion and photon echo experiments, and *ab initio* calculations performed in our group within the last few years with respect to the light harvesting process in purple bacteria. Carotenoids transfer energy to bacteriochlorophyll (BChl) mainly via the carotenoid $S_2 \rightarrow$BChl Q_x pathway on a ~ 100 fs timescale. This transfer is reasonably reproduced by considering the Coulombic coupling calculated using the transition density cube method which is valid at all molecular separations. Carotenoids may also serve a role in mediating B800 $\rightarrow$B850 energy transfer in LH2 by perturbing the transition density of the B850 as shown by *ab initio* calculations on a supermolecule of two B850 BChls, one carotenoid and one B800 BChl. Further calculations on dimers of B850 BChl estimate the intra- and interpolypeptide coupling to be 315 and 245 cm^{-1}, respectively. These interactions are dominated by Coulombic coupling, while the orbital overlap dependent coupling is $\sim 20\%$ of the total. Photon echo peak shift experiments (3PEPS) on LH1 and the B820 subunit are quantitatively simulated with identical parameters aside from an energy transfer time of 90 fs in LH1 and ∞ in B820, suggesting that excitation is delocalized over roughly two pigments in LH1. 3PEPS data taken at room and low temperature (34 K) on the B800–B820 suggest that static disorder is the dominant mechanism localizing excitation in LH1 and LH2. We suggest that the competition between the delocalizing effects of strong electronic coupling and the localizing effects of disorder and nuclear motion results in excitation in the B850 and B875 rings being localized on 2–4 pigments within approximately 60 fs.

PACS numbers: 87.15.Mi, 82.20.Rp, 42.50.Md

1. Introduction

The primary events of photosynthesis consist of two processes — light harvesting and charge separation. The former takes place in antenna or light harvesting complexes while the latter occurs in reaction centers [1–3]. In this article we will focus on the light harvesting process in purple bacteria, using the 2.5 and 2.4 Å resolution structures of the light harvesting 2 complexes (LH2) from *Rhodopseudomonas (Rps.) acidophila* [4] and *Rhodospirillum (Rs.) molischianum* [5] as guides to explore the way in which chromophore–chromophore and chromophore–protein interactions are used to construct a broadband antenna capable of directing excitation energy to the reaction center with near unit efficiency. Our strategy is to combine ultrafast spectroscopy, in particular photon echo spectroscopy and fluorescence upconversion spectroscopy, with electronic structure calculations and theory to explore the physics underlying these remarkably efficient and beautiful structures.

Energy is transferred preferentially toward the reaction center partly by means of a downhill energy "funnel". LH2 is the outer antenna and consists of bacteriochlorophyll *a* molecules (BChl) absorbing at 800 nm (B800) and at 850 nm (B850). The reaction center sits within a second complex — LH1 — consisting of BChl molecules absorbing at 875 nm (B875). Both antenna complexes are highly symmetric ring structures based on self-assembled repeats of $\alpha-\beta$ polypeptides with 8 (*Rs. molischianum* [5]) or, 9 (*Rps. acidophila* [4]) fold symmetry in LH2, or 16 fold symmetry for the LH1 complex [6]. The LH2 structure, taking the *Rps. acidophila* structure for the sake of definiteness, contains 9 B800 BChls and 18 B850 BChls [4]. Although the structural information for LH1 is much less detailed, it seems highly likely that the 32 B875 BChls are arranged in a similar manner to the B850 BChls of LH2. Figure 1 summarizes the layout of the reaction center/LH1/LH2 system, called the photosynthetic unit (PSU) [7]. The repeating units of α and β polypeptides with their associated pigments are referred to as protomer units. Interactions between pigments in the same (different) protomer unit are termed intra(inter)polypeptide.

The structure of LH2 shows that the B850s are in much closer contact than the B800s suggesting that the shift from 800 nm to 850 nm results from excitonic coupling between the B850 molecules. However mutant studies suggest that hydrogen bond interactions with tyrosine and tryptophan residues in the protein are responsible for about half the total shift [8]. As we will show later, our electronic structure calculations strongly support the picture of protein-induced transition energy shifts and provide a clear example of protein involvement well beyond that of an inert scaffold for the chromophores.

The LH2 structure also reveals the remarkably intimate interaction of the carotenoid molecules, rhodopin glucoside (RG), with all the BChls [4, 9, 10] (Fig. 2). These long-chain polyenes play numerous roles in photosynthesis. The primary role is photoprotection by removal of BChl triplet states, thereby avoiding singlet oxygen generation [11, 12]. With very few exceptions, all chlorophylls in photosynthesis in both plants and bacteria are protected by carotenoids. One significant exception is the primary electron donor of Photosystem II (P680). P680+
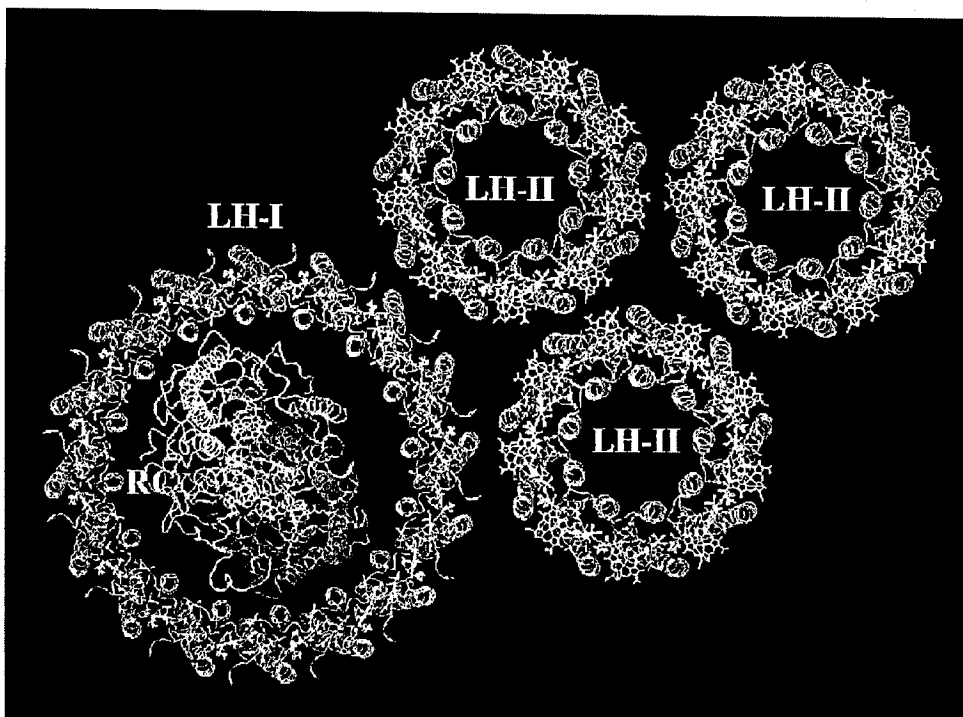
Fig. 1. A model for the photosynthetic unit (PSU) of *Rb. sphaeroides*. The α polypeptides of both LH1 and LH2 are blue while the β are magenta. The L, M and H subunits of the RC are yellow, red and gray, respectively. All BChls are green and carotenoids are yellow. Three LH2 rings are shown, but the actual number of LH2 rings per PSU is probably variable and may be as high as ten in *Rb. sphaeroides*. This model was generously provided by Xiche Hu (see Ref. [7]).

is such a strong oxidizing agent ($E_0 \approx 1.2$ V) that any adjacent carotenoid would be oxidized in preference to the correct electron donor (a tyrosine residue [13, 14]). Thus damage to PSII is unavoidable and dismantling and reassembly part of its normal function [15–17].

In addition to photoprotection carotenoids play structural roles [11, 12] and provide, in many species, additional light harvesting from the region of the spectrum where BChl (or Chl) absorption is weak. The efficiency of light harvesting from carotenoids is generally > 90% in purple bacteria and is $\sim$ 100% in *Rhodobacter (Rb.) sphaeroides* [18]. Such efficiency is impressive, especially given that the S_1 state of carotenoids is optically dark and thus initial absorption is to the S_2 state. Further, the extended nature of the carotenoid and the proximity to neighboring pigment molecules make simple (e.g. point dipole) treatments of the energy transfer inappropriate. To deal with such a system we have developed a new method — the transition density cube method — for the calculation of Coulombic energy transfer [19]. The method is formally exact and fully 3-dimensional. We provide details of the carotenoid–BChl energy transfer in the next section. Following this,
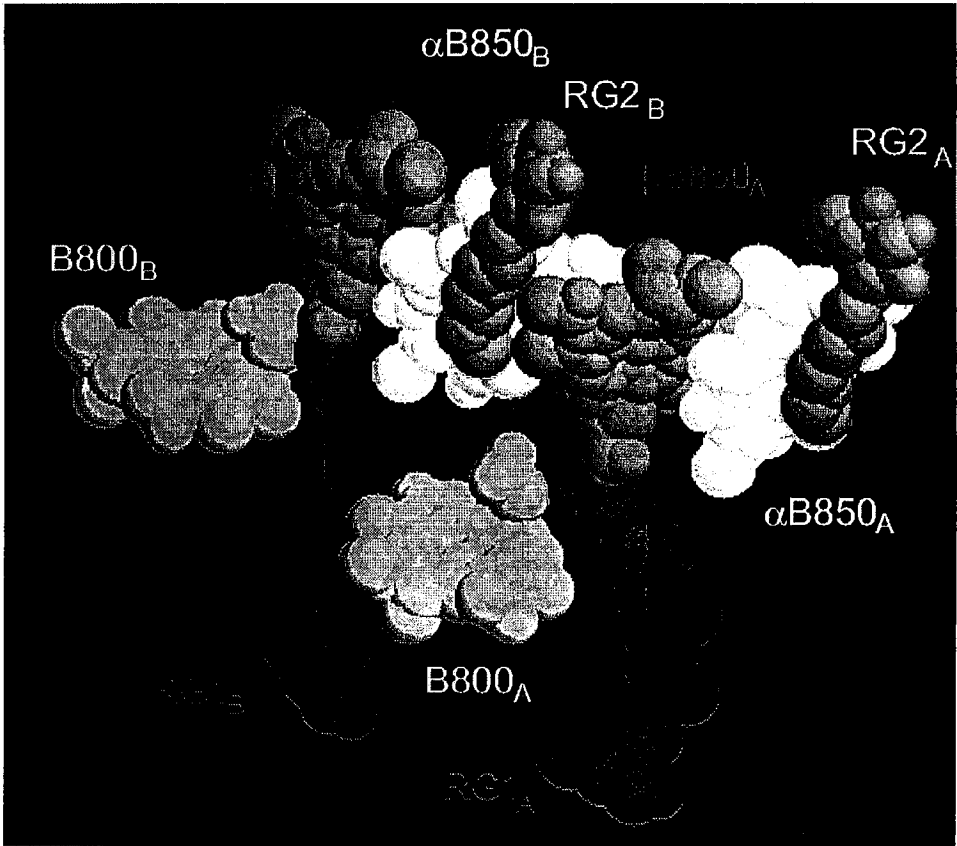
Fig. 2. A portion of the LH2 ring of *Rps. acidophila* including four B850 BChls (α: light blue and β: purple), two RG carotenoids (red) and two B800 BChls (green). Also shown are two molecules labeled RG2 (orange) which may be partially resolved carotenoids [4]. The polypeptides are not shown and the phytyl chains of the BChl have been removed for clarity. The α and β labels differentiate the two types of B850 according to which polypeptide they are bound, while the A and B labels denote different protomer units (as in Ref. [19]). An example of an intrapolypeptide B850 pair is the αB850$_A$ and βB850$_A$; an interpolypeptide pair is the βB850$_A$ and the αB850$_B$.

we discuss the possible role of the carotenoid in the B800 to B850 energy transfer in LH2. In Sec. 3 we discuss energy transfer within LH1 and in the B850 ring of LH2. We also provide results of electronic structure calculations on dimers of B850 molecules to obtain estimates of the Coulombic and orbital overlap contributions to the electronic coupling. B850 dimer calculations with and without hydrogen bond interactions with the tryptophan and tyrosine residues show the influence of proteins on the electronic structure. Finally Sec. 4 presents some concluding remarks.

2. The role of carotenoids in energy transfer

As remarked earlier, the first excited singlet state of carotenoid molecules is an optically dark A_g symmetry state. The S_0-S_2 transition is strongly allowed but as Fig. 3 shows the S_2 lifetime is very short ($\sim$ 250 fs) in solution. However as Fig. 3 demonstrates, the lifetime is even shorter in intact LH1 and LH2 complexes ($\approx$ 55–90 fs, depending on species and specific carotenoid involved). This shortening could simply be enhanced $S_2 \rightarrow S_1$ internal conversion, rather than energy transfer. However, detailed analysis of the data shown in Fig. 4 where the rise of the BChl Q_y emission is recorded in the same sample as the S_2 fluorescence decay, shows that the majority of RG $\rightarrow$ BChl transfer occurs via $S_2(\text{RG}) \rightarrow Q_x(\text{BChl}) \rightarrow Q_y(\text{BChl})$ with a rate of 1.1×10^{13} s^{-1} for the first step [20]. Is such a rapid energy transfer process compatible with standard Coulombic coupling theory as exemplified by Förster [21] theory? To address this issue we calculated *ab initio* transition densities [19] for the RG, and for several BChls of the *Rps. acidophila* LH2 structure at the 3–21G* level. Figure 5 shows the RG transition density — its lack of resemblance to a point hardly needs emphasis. However, it may be worthwhile mentioning the advantages of the transition density cube (TDC) method (illustrated in Fig. 6) over the point monopole method introduced in the 1940's [22–24] and applied to problems of energy transfer (electronic coupling) by a number of authors [25–27]. The TDC method is formally exact limited only by the quality of the wave functions. The point monopole approximation is not exact (and in fact is quite poor for the RG–BChl interaction),
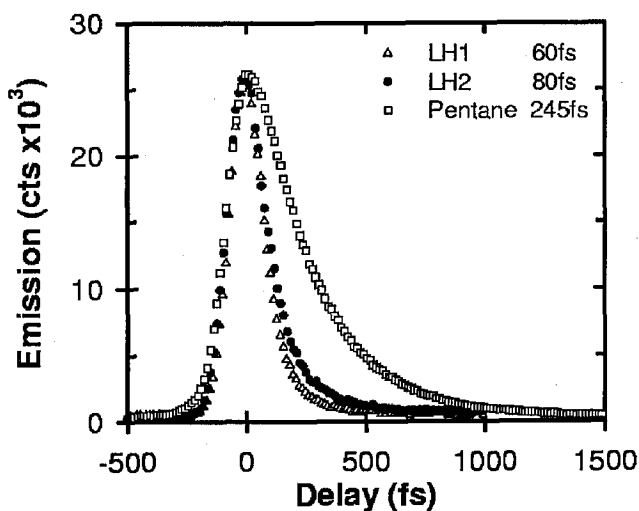
Fig. 3. Fluorescence upconversion data of emission from the S_2 state of the carotenoid spheroidene in *n*-pentane solution ($\square$) and in the light harvesting complexes LH1 ($\triangle$) and LH2 ($\bullet$) of *Rb. spheroides*. The lifetimes of the decays are 245 fs in pentane, 80 fs in LH2 and 60 fs in LH1.
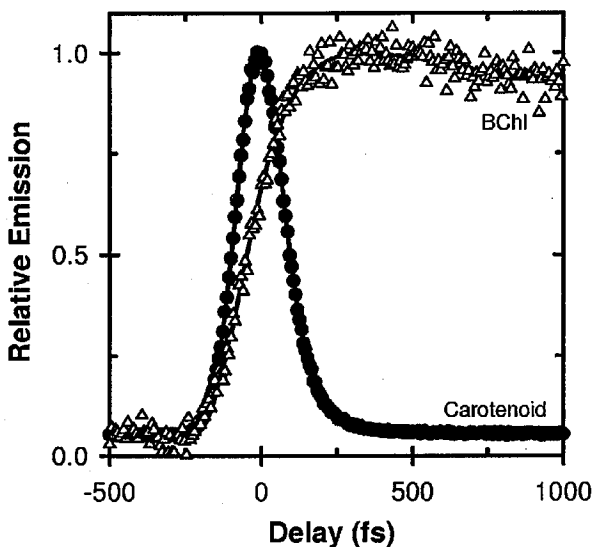
Fig. 4.   Fluorescence upconversion data and fits from the B800–B820 LH2 complex of *Rps. acidophila* showing the decay in emission from the S_2 state of the carotenoid ($\bullet$), RG, and the rise in emission from the Q_y state of the B820 BChl ($\triangle$) following excitation into the carotenoid S_2 state. The lifetime of the carotenoid decay is ~ 55 fs and of the BChl rise is 110 fs. Wavelength dependence of the BChl rise time is not shown.
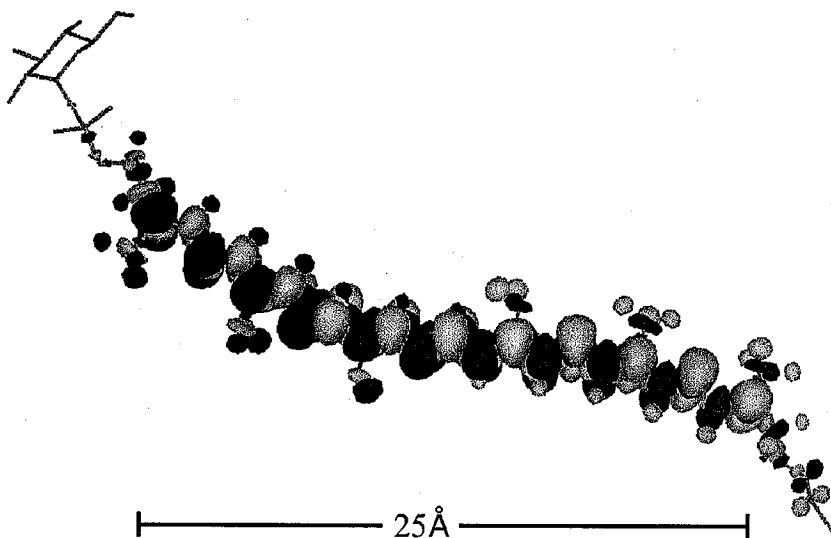
Fig. 5.   Transition density of the carotenoid, RG. The shape of the carotenoid is taken from the crystal structure [4] and the transition density is determined as described by Krueger et al. [19].
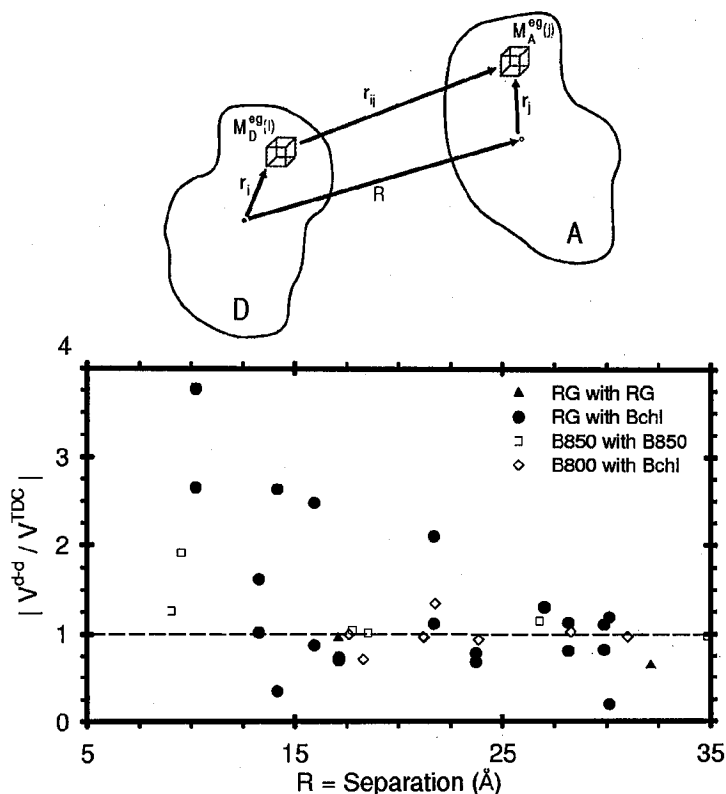
Fig. 6.   (top) Transition Density Interaction Scheme. Depiction of two cells in arbitrary donor (D) and acceptor (A) transition densities. The positions of the TDC elements $M_D^{eg}(i)$ and $M_A^{eg}(j)$ are given by vectors r_i and r_j, respectively, relative to the centers of D and A. $\mathbf{R}$ gives the center to center separation and r_{ij} the separation between cells. Note that because the interaction is summed over all i and j, the total interaction is independent of the positions of the centers of D and A. (bottom) Deviation between the actual Coulombic coupling calculated using the TDC method, V^{TDC}, and the dipole–dipole approximation to it, V^{d-d}, plotted as the ratio $|V^{d-d}/V^{TDC}|$ versus the center to center separation for various pigments in LH2.

and suffers from the standard ambiguity of assigning partial charges to nuclear centers in a molecule [28]. Even if, say, one adopts Mulliken partial charges as a "standard", ground and excited state wave functions are still required, so the exact TDC interactions can be directly calculated, rather than reducing the transition density to an approximate, monopole representation. Thus there are significant advantages to the TDC approach.

Figure 6 compares "exact" Coulombic couplings with those obtained from point dipole calculations for various RG–BChl and BChl–BChl interactions in LH2. For couplings involving the RG molecule, the point dipole approximation
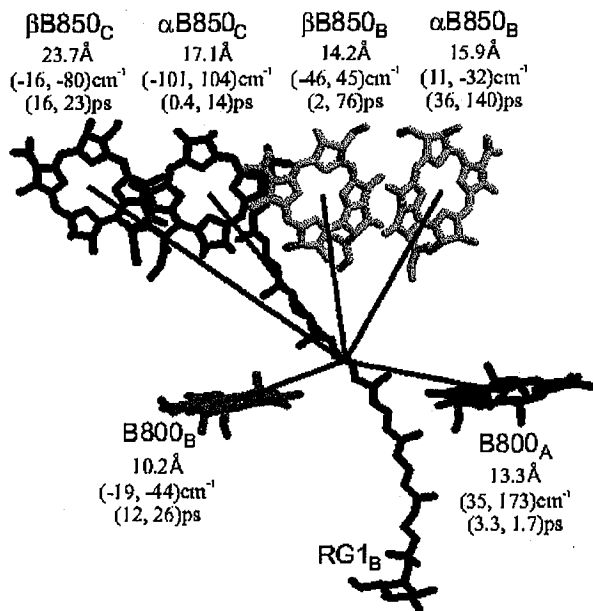
Fig. 7. Coupling strengths and energy transfer times from the RG1$_B$ S$_2$ transition to nearby BChl transitions. Near each acceptor pigment is given the label, center to center separation, coupling strength from the TDC calculation, and transfer time. Coupling strengths and transfer times are given for interaction with both the Q_x and Q_y transitions of the BChl as (Q_x, Q_y).

can be in error even at center to center separations greater than 25 Å. At smaller separations, errors become severe (recall rates are proportional to the square of the coupling). Figure 7 shows calculated rates of energy transfer from RG to several B850s and also to B800 in LH2. Rates are given for both Q_x and Q_y transitions of BChl, calculated by evaluating spectral overlap factors for each process [20]. Figure 7 shows that the sum of rates from the RG molecule is comparable to the total decay rate obtained in Fig. 4 (and by others [29, 30]) and is dominated by the 0.4 ps S_2(RG1$_B$) → Q_x(αB850$_C$) transfer, although others, notably S_2(RG1$_B$) → Q_x(βB850$_B$) and S_2(RG1$_B$) → Q_x and Q_y(B800$_A$), are also significant and lead to a total RG S_2 → BChl transfer time of ~ 230 fs [19]. Bear in mind that, despite this rapid energy transfer, S_2 → S_1 internal conversion is likely the single most rapid process depopulating the S_2 state.

Although the agreement between calculated and measured rates is satisfactory, it is unlikely that Förster theory in its simplest form with time independent spectral overlap factors applies directly. Indeed we see changes in the kinetics recorded at different wavelengths in the B850 Q_y transition, consistent with emission from vibrationally unrelaxed molecules on the few hundred fs timescale. A model incorporating time dependent overlap has been described by Mukamel [31] but we have not pursued it in this work. In the case of carotenoid S_2 → B850 Q_x transfer the effect of time dependent overlap on the total rate is unlikely to be

large because the carotenoid S_2 emission is very broad compared to the BChl absorption.

This broad spectrum is a key reason for the success of carotenoids as light harvesting pigments. The S_2 absorption is strong over a wide wavelength range (~ 100 nm) making it an efficient collector of sunlight. The carotenoid emission is also broad giving it significant spectral overlap with potential acceptor pigments (BChl) across a wide range in energies. Thus, the carotenoid is well suited to be an energy donor in light harvesting antenna which are composed of several spectral types of BChl, which are each inhomogeneously broadened. Carotenoid $\rightarrow$ BChl energy transfer efficiency is also improved by the structure which allows several potential BChl acceptors to couple strongly with the RG (see Fig. 7). Moderately fast energy transfer from one carotenoid to each of several possible BChl results in a total process that exceeds efficiencies of 90% in many bacteria [18].

Jimenez et al. show upconversion data (in their Fig. 2) for B800–B850 energy transfer [32]. This may seem an odd topic for a section devoted to carotenoids. However, various lines of evidence are beginning to suggest that the carotenoid
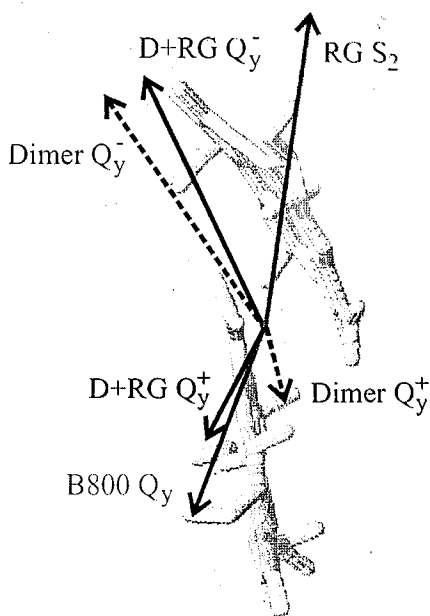
Fig. 8. Transition densities, reduced to transition dipoles, of the two Q_y transitions (upper Q_y^+ and lower Q_y^-) from the B850 interpolypeptide dimer both with (D+RG) and without (Dimer) the presence of the carotenoid. All dipoles are shown projected into the plane of the membrane and originating from a point midway between the centers of the B850 BChls. The lower transition (with most of the oscillator strength) from the B850 pair is red and the upper is blue. Results of the dimer-only calculation are given by dotted lines while those from the full "supermolecule" calculation are given by solid lines. Transition moments for the carotenoid (purple) and B800 BChl (green) are given for reference.

molecule is directly involved in the B800–B850 transfer in at least two ways. Attempts to calculate the rate of B800–B850 transfer from Förster theory — which in the absence of the carotenoid should be very accurate at this separation (> 17 Å), even for point dipoles (cf. Fig. 6) — always produce rates that are too slow (~ 2 ps [19, 32, 33] vs. the observed 650–700 fs [32, 34]). (Note that Ref. [19] reports a calculated transfer time of 1.3 ps which is an error. $B800_A - \beta B850_B$ coupling should be 2.3 cm^{-1} rather than the stated 23 cm^{-1}, which brings the total B800–B850 transfer time to 1.8 ps rather than 1.3 ps.) Various suggestions have been made to account for this difference, including the involvement of the upper exciton transition expected for the interaction of two B850 molecules. Our electronic structure calculations involving a "supermolecule" of two B850s, RG, and B800 suggest a more sophisticated model. Examination of HOMO and LUMO molecular orbitals for this supermolecule show clear evidence for mixing of the RG S_2 state with the B850 molecules [35]. No orbital mixing is observed between the RG and the B800 molecule, though calculations have been completed for only one of the two possible B800s. The RG/B850 mixing can clearly enhance the B800–B850 transfer by (1) drawing transition density closer to the B800 and (2) by altering the direction and magnitude of the relevant transition moments on B850. Our *ab initio* calculations strongly imply that both effects occur. Figure 8 shows projections of the B850 transition dipoles, calculated both with and without the carotenoid, onto the membrane plane. This 2-dimensional picture is not quantitative, but it clearly shows that the carotenoid has a significant influence on the direction of the B850 transition dipoles. The results of TDC calculations quantifying this effect will be reported elsewhere [35].

3. Energy migration within B850 and within B875

The nature of the electronic states and the mechanism of energy transfer within the B850 and B875 rings of LH2 and LH1, respectively, has been debated extensively [27, 32, 36–45]. Models ranging from complete electronic delocalization on all timescales to localized hopping between dimers on a 100 fs timescale have been described [27, 32, 39, 44, 45]. In order to provide a realistic description of such a system a number of ingredients are required: (1) the strength of electronic coupling between B850 or B875 molecules, (2) the magnitudes and timescales of the electron–phonon coupling contributions, (3) the timescale of energy transfer within the ring, and (4) the magnitude of the disorder in both diagonal (i.e. transition energy) and off-diagonal (i.e. coupling) energies. Several factors contribute to the wide range of opinions expressed in the literature. First, the full problem is very complex and simplified models can be quite misleading. Second, ultrafast nonlinear spectroscopy, particularly in the form of photon echo spectroscopy, has been very successful in revealing electron–phonon coupling in dilute chromophore systems, but has not been especially incisive in delineating electronic interactions in more complex systems. Further, the theoretical basis for techniques such as the photon echo peak shift when applied to molecular aggregates has not until recently been fully developed [46, 47] and the models used to interpret the data may be oversimplified. Additionally, while strong evidence exists that LH1 and LH2 are disordered, the presence of energy transfer makes it difficult to measure

the magnitude of the energetic disorder directly as has been done, for example, for dilute solutions of dyes in polymer glasses [48]. Finally, a basic exciton model of the electronic states of such a system is undoubtedly oversimplified. It neglects the role of the medium in modifying chromophore properties and, by ignoring orbital overlap effects in the interchromophore coupling, is likely to err on the relative locations of 1- and 2-exciton states — a property of considerable significance in interpreting transient absorption measurements [49].

These considerations led us to a combined *ab initio* electronic structure/photon echo approach. Properly interpreted, the photon echo peak shift method (3PEPS [50–52]) can provide quantitative information on points (2)–(4) above (with the exception of the coupling disorder) while the electronic structure work should provide accurate couplings and a realistic model for the electronic states and transition moment directions of the complex (1). Taken all together these inputs should enable a complete model for the dynamics to be constructed.

We first turn to a description of the photon echo data. Figure 9 compares photon echo peak shift data for LH1 with that for a dilute solution of the dye IR144 in the polymer glass PMMA. Detailed descriptions of the 3PEPS method
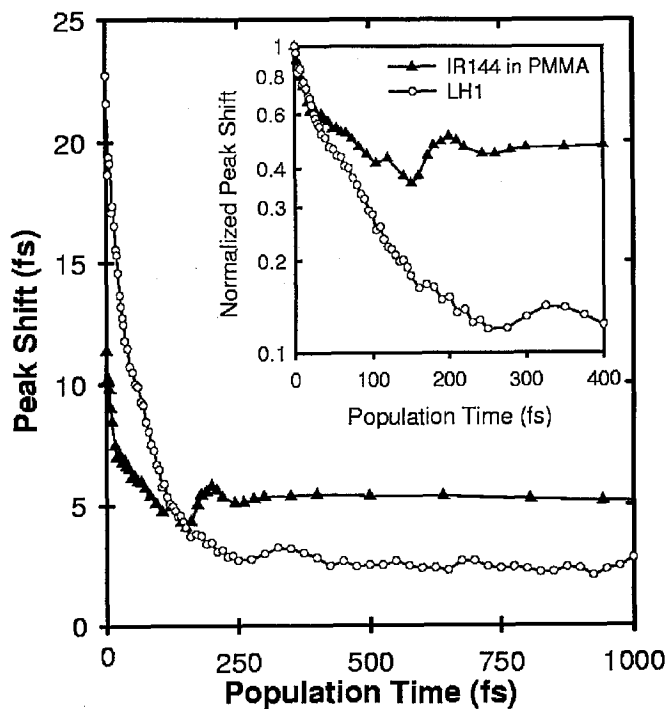
Fig. 9.   Photon echo (3PEPS) data for B875 BChl in LH1 (o) and for IR144 in PMMA (full △). In the inset, the data have been normalized to their initial values and plotted on a logarithmic scale.

and its information content can be found in Refs. [47, 51, 52]. Here we simply emphasize a few key points. Two striking differences between the IR144/PMMA and LH1 data sets are immediately obvious in Fig. 9. The initial peak shift in LH1 is much larger than that of the dye. This implies a very weak electron–phonon coupling in the light harvesting complex since, over a reasonable parameter range, the initial peak shift is roughly inversely proportional to the total coupling strength of the transition to nuclear degrees of freedom. Second, as the inset makes clear, the IR144/PMMA data become independent of population time (T) after about 200 fs whereas the LH1 data continue to decay and, in fact, the peak shift is zero at about 15 ps. A finite long time peak shift definitely signals static (on the experimental timescale) inhomogeneous broadening of the optical transition energies. Conversely, a zero value of the peak shift indicates that the ensemble is homogeneous on that timescale and is typically observed for dilute chromophores in fluid solutions on the 5–50 ps timescale.

Do the data imply absence of a distribution in transition energies in LH1? On the contrary, we interpret the LH1 3PEPS data to imply effective averaging over the distribution as a result of the energy transfer around the LH1 ring. Thus the energy transfer timescale should be present in the LH1 data and, as described below and elsewhere [47], it is possible to derive a simple model for the peak shift which contains a term $\Delta_{in}^2 \exp(-t/\tau_{ET})$ where Δ_{in} is the width of the inhomogeneous distribution and τ_{ET} is the energy transfer time constant. Applying this model to LH1 and LH2 peak shift data yields energy transfer timescales of 90 fs and 130 fs, respectively [53], consistent with earlier estimates from upconversion data [32, 39] and pump-probe studies [41, 42, 54–56]. As a check on the basic concept of this analysis — that the peak shift directly reflects energy transfer despite the technique's insensitivity to population dynamics in dilute two-level systems — 3PEPS measurements were made on the B820 subunit of LH1 [38]. The B820 subunit consists of a single pair of "B875" molecules [57] and is thus incapable of long range energy transfer. In line with this expectation, the peak shift shows a finite long time value just as for the dilute dye in polymer glass case. In addition, the initial peak shift increases slightly as compared to LH1. Thus the simplest model for B820 3PEPS data would be to take the parameters obtained for LH1 and, keeping all the electron–phonon coupling constants the same, simply set $\tau_{ET} = \infty$ in the energy transfer contribution to the total response. Note that this term is not removed — it simply becomes Δ_{in}^2. As described elsewhere [38], this procedure is extraordinarily successful. The finite long-time peak shift is quantitatively recovered suggesting that Δ_{in} is identical in LH1 and its B820 subunit. The initial dynamics (arising from vibrational and protein motions) are also quantitatively reproduced and the increase in initial peak shift is predicted correctly since the ratio of static to dynamic broadening has changed in the absence of energy transfer. This success, despite the caveats listed below, strongly suggests that a reasonable working model for the electronic structure of LH1 — and by extension possibly for LH2 also — is of dimeric BChl subunits. This suggests that even at 300 K disorder is playing the dominant role in localizing the electronic states [58, 59]. An important way to check this is by carrying out 3PEPS experiments as a function of temperature. This we have done for a different strain of *Rps. acidophila*

than we have discussed so far — strain 7050. In this LH2 complex, hydrogen bond interactions between the B850 BChls and residues αTyr44 and αTrp45 are lacking, affecting the angle of the acetyl carbonyl group relative to the BChl ring — blue-shifting the Q_y transition [60]. It consequently exhibits absorption bands at 800 and 820 nm and is referred to as B800–B820. The B820 molecules are otherwise structurally equivalent to the B850 BChls discussed above.
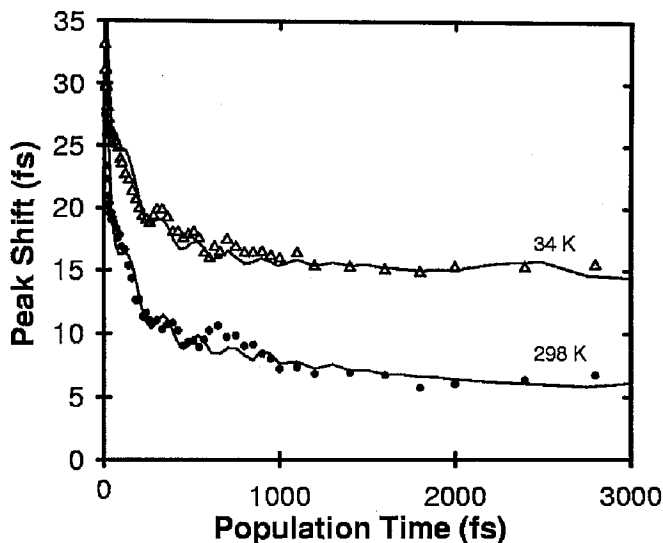
Fig. 10. Temperature dependent 3PEPS data from the B800–B820 LH2 complex from *Rps. acidophila*. Room temperature (298 K) data are given by circles (•) and low temperature (34 K) by open triangles ($\triangle$); simulations of the data are given by the solid lines.

Figure 10 shows 3PEPS data at 298 K and 34 K for the B820 component of B800–B820 with simulations. The data are analyzed with the same model as discussed above with one addition. Even at 298 K there is a small constant peak shift at long times in B800–B820. This suggests that some subset of the molecules are inaccessible via energy transfer, presumably because the inhomogeneous distribution is wide enough compared to the ~ 200 cm^{-1} thermal energy that a small number of sites are effectively isolated in this sample. Analysis of the data reveals that, though the amount of the inhomogeneous distribution sampled by the energy transfer changes with temperature from $\sigma = 100$ cm^{-1} at room temperature to $\sigma = 60$ cm^{-1} at 34 K, the total width of the inhomogeneous distribution is temperature independent ($\sigma = 120$ cm^{-1}).

The couplings between BChl a chromophores which comprise the B850 ring of LH2 (*Rps. acidophila*) were calculated recently using *ab initio* methods [61]. Electronic couplings were estimated from "supermolecule" calculations of BChl dimers using the CI-singles methodology and 3–21G* or 6–31G* basis sets. A scheme for dissecting the coupling into contributions from the Coulombic coupling

and the short-range coupling (i.e., dependent on interchromophore orbital overlap) was reported. The results are summarized in Table I. The Coulombic coupling, V^{Coul}, provides the largest contribution to the total couplings. It is found to be insensitive to basis set. As anticipated, the dipole approximation does not reproduce the V^{Coul} for the B850 couplings. It is evident from Table I that the contribution to the couplings from orbital overlap-dependent interactions (short range coupling, V^{short}) is fairly small compared to V^{Coul}. Similar short-range couplings contribute to both the interpolypeptide coupling and to the intrapolypeptide coupling. We conclude that the orbital overlap-dependent contribution to the coupling for both the intra- and interpolypeptide dimers is at least 60 cm^{-1}. This represents approximately 20% of the total coupling. To put this in perspective, it is at least twice the magnitude of the total B800–B800 coupling.

TABLE I

Calculated couplings (CIS/3–21G*) for the intrapolypeptide and interpolypeptide dimers (see Fig. 2) of the B850 ring of LH2 (*Rps. acidophila*) both without and with the influence of Tyr, Trp and His residues. V^{total} is dissected into the Coulombic and short-range contributions. The dipole–dipole coupling, V^{d-d}, is given for comparison. Couplings are quoted in cm^{-1}.

Dimer	V^{total}	V^{Coul}	V^{short}	V^{d-d}
Intra ($\alpha_A - \beta_A$)	315	270	45	415
Inter ($\beta_A - \alpha_B$)	245	205	40	330
Intra (with residues)	335	230	105	395
Inter (with residues)	295	180	115	320

Repeating these dimer calculations, but including the hydrogen bonding residues αTyr44 and αTrp45 along with αHis31 and βHis30 which ligate the central magnesium of the α and βBChl result in slightly different coupling strengths. The new intra- and interpolypeptide couplings are 335 and 295 cm^{-1}, respectively. Also, in the absence of protein, the βB850 transition energy is lower in energy than the αB850 because it has a slightly bent conformation (raising the energy of the ground state versus the excited state). Inclusion of the protein residues reduces this transition energy difference, providing for stronger interaction between the BChls. In addition, calculations with and without the hydrogen-bonding residues quantitatively reproduces the red shift from 820 to 850 nm found by site-directed mutagenisis studies [8].

The small B800–B800 coupling (in excellent agreement with V^{d-d}) is consistent with an incoherent hopping (i.e. Förster [21]) model for intraband energy transfer [62]. However, it is thought that for B850 the couplings are of the same magnitude as the disorder (inhomogeneous broadening) and the homogeneous linewidth. Hence, a simple Förster model should be inapplicable. In previous work the energy migration in B850 has been modeled as hopping between

dimers [32]. In that work it was found that the fluorescence depolarization kinetics could be modeled by assuming an intrapolypeptide coupling of 230 cm^{-1}, an interpolypeptide coupling of 110 cm^{-1}, and a site disorder of 200 cm^{-1}. It was suggested that the resultant dynamics could be described as incoherent hopping between dimers [32, 39, 63] (prompted by the strong interactions evident in the B820 dimeric subunit of LH1 [64–68]), however the authors emphasized that electronic structure calculations were necessary to confirm the speculation. Superradiant fluorescence emission (i.e., enhanced radiative rates of a molecular aggregate compared to a monomer [69]) have been studied recently in LH2 and LH1 of *Rb. sphaeroides* [40]. Since the superradiance characterization requires steady state quantum yield data, this measurement provides information only on the long time delocalization. An enhancement of the radiative rate of B850 of 2.8 times that of monomeric BChl *a* at room temperature was reported. We find from analysis of the molecular orbital calculations that the superradiance electronic enhancement factors for the intra- and interpolypeptide dimers, $K = k_{\text{rad}}^{\text{dimer}}/k_{\text{rad}}^{\text{monomer}} = f^{\text{dimer}}/f^{\text{monomer}}$, are approximately 2.1 and 1.9, respectively (assuming an average monomer oscillator strength of 0.7). A relatively small contribution from short-range interactions was surmised. Pullerits et al. [37] have simulated fs transient absorption experiments of the B850 region after excitation of the B800 band and subsequent energy transfer to B850. Their results suggest a delocalization length of 4 ± 2 molecules. Kennis et al. [58] have employed fs transient absorption measurements to compare B850 with the special pair of the reaction center, and conclude that the delocalization length in B850 is 2.5 molecules at 5 K.

A key parameter required for the detailed analysis of spectroscopic data of molecular aggregates such as LH1 and LH2 is the electronic coupling. Mukamel and coworkers have recently described a method of analysis of photon echo data based on the density matrix, which requires input of disorder, site spectral densities, geometry of the aggregate and electronic couplings. Consideration of the LH1/B820 results and analysis suggests that a number of open questions regarding the elucidation of energy transfer dynamics via 3PEPS data remain. Now that we have calculated the electronic couplings in LH2, we are in a position where we can begin to calculate the dynamics of energy transfer, and simulate our 3PEPS data. However, as shown by Mukamel and co-workers [46, 70], this is complicated owing to the multiple electronic states in resonance with the excitation pulses. Population redistribution amongst these levels occurs during the population period (energy transfer) and many-body effects contribute to dephasing during the coherence periods. Moreover, at times less than approximately 150 fs, there may be a significant contribution to the 3PEPS signal from a ground state bleaching term ($R^{(b)}$) and a coherent term ($R^{(c)}$), which involves no contribution from (bath-mediated) population relaxation amongst the zero-order electronic levels. These terms involve the aggregate two-exciton electronic states; that is, the possibility that pathways involve excitations on different (but electronically coupled) chromophores in the aggregate. The time-domain optical response function which relates the third-order nonlinear polarization to the driving field is written as:

$$R(t_3, t_2, t_1) = R^{(b)}(t_3, t_1) + R^{(c)}(t_3, t_2, t_1) + R^{(\text{pop})}(t_3, t_2, t_1). \tag{1}$$

The possibility of double excitation of one molecule was not included in the theory, but this is a distinct possibility in the case of BChl aggregates, since BChl has a strong excited state absorption at a very similar wavelength to its ground state absorption [71]. Moreover, the theory was derived under the assumption of a Frenkel model for the aggregate electronic states. This should be a good approximation for aggregates which are comprised of molecules which do not share electron density (i.e., their orbitals do not overlap). However, we know from our *ab initio* molecular orbital calculations of the electronic couplings that this is not the case for the B850 ring of LH2. In model calculations the peak shift was found to be significantly diminished at population times greater than zero as a direct result of the $R^{(b)}$ and $R^{(c)}$ contributions to the overall signal. However, this effect may be significantly reduced by the spectral shifts associated with the orbital overlap-dependent couplings.

The final term of Eq. (1) describes energy transfer during the population period. Owing to the timescale separation between slow dynamical variables (the evolution of single exciton populations) and the fast dynamical variables (bath fluctuations), it can be written in the form

$$R^{(\mathrm{pop})}(t_3, t_2, t_1) = \sum_{\mu\nu} D_\nu(t_1) G_{\mu\nu}(t_2) W_\mu(t_3). \tag{2}$$

The first contribution on the right hand side, $D_\nu(t_1)$, is the doorway function which represents the population of the ν-th exciton state after two interactions with the radiation field (two interactions are needed to create a population state, i.e., to excite the sample). Given the separation of timescales defined above, this term essentially dictates the degree to which the population density is localized upon excitation. We discuss this further below. The final contribution to Eq. (2) is the window function, $W_\mu(t_3)$, which represents the contribution of the μ-th exciton state to the signal.

The evolution of population between the second and third pulses (called the population period, T) is described by $G_{\mu\nu}(t_2)$. It represents the conditional probability for the population of the ν-th exciton state to migrate to the μ-th exciton state, as described by a Master equation. As discussed below, we believe that excitation in photosynthetic antenna systems is more localised, with respect to antenna size, than delocalized. In other words, $D_\nu(t_1)$ creates a relatively localized excited state population density; thus a physical picture of the population evolution during T is that of energy transfer between quasi-localized sites (i.e., each site may correspond to more than one chromophore). (Note that this physical picture is introduced for convenience only — formally the theory is equivalent for either site or eigenstate representations.) The theory described by Zhang et al. [46, 70] for the nonlinear response of molecular aggregates thus deals explicitly with the dynamics in the excited state population pathway (labeled *ee* in the usual notation). Though it is not discussed by Zhang et al., the description of the evolution of the excited state pathway also applies to the ground state pathway (labeled *gg*) which also leads to generation of an echo. It is not obvious that a mechanism of energy transfer averaging over the inhomogeneity should apply to ground state contributions as well as to excited state contributions. However, this is indeed the

case. As excitation migrates from site to site, the *ee* contributions sample the inhomogeneous distribution. As sites are de-excited, they become members of the ground state pathway and sample the inhomogeneity in the same way.

We now consider the doorway function, which is an important part of Eq. (2) since it sets up the excited state population in terms of its initial, and dominant, extent of localization (given the separation of dynamical timescales defined by Zhang et al.). It is defined as

$$D_\nu(t) = -\mu_\nu^2 \left\{ \exp[-i\varepsilon_\nu t - g_{\nu\nu}(t)] + \exp\left[i\varepsilon_\nu t - g_{\nu\nu}(-t)\right] \right\}, \tag{3}$$

for exciton state ν with excitation energy ε_ν and dipole transition moment μ_ν. The $g_{\nu\nu}(t)$ is the line-shape function for the eigenstate ν. It is evident that there is some analogy between the doorway function and the absorption line-shape. Furthermore, the form of the aggregate line-shape function indicates that if the energy gap correlation function is $M(t)$ for one site, then for an eigenstate of N identical molecules, it is approximately $\sqrt{N}M(t)$. Though this does not effect the time-dependence of the 3PEPS signal, it does impact the overall magnitude of the peak shift (i.e., the total coupling extracted from simulations). If the static and dynamic influences on localization are strong enough, partial localization may occur during the preparation (doorway) step.

Given the timescales measured in 3PEPS and other experiments and the coupling strengths from our electronic structure calculations, we can begin to piece together a description of the dynamical localization occurring in LH2 which we compare to recent density matrix calculations by Kühn and Sundström [59]. The only process which delocalizes the excited state density matrix is the electronic coupling given in Table I. Kühn and Sundström show that under delocalization-only conditions, the exciton is completely delocalized, as expected, over all timescales. Consideration of the localization effects of the static disorder yields a timescale of ~ 60 fs, obtained through the empirical model of Kumble and Hochstrasser [49] using site inhomogeneity of $\sigma = 170$ cm^{-1} [53], and coupling strength of 300 cm^{-1}. In Ref. [61] the same competing factors of electronic coupling and static disorder were used to calculate the absorption spectrum and degree of localization for B850. This gives an estimate of the delocalization length of approximately four to six BChls. In addition, all nuclear motions also act to localize the excitation. Both intra- and intermolecular contributions to the dephasing act with timescales of 40–70 fs. Considering the additional localization effect of all these nuclear timescales, it is probable that the number of BChl molecules in B850 over which some degree of electronic coherence can be maintained is between two and four. Assuming a model for LH2, Kühn and Sundström show that significant localization does occur during the preparation step, and that at long times, the exciton is delocalized over 4 ± 2 pigments [37, 59]. The picture which emerges is that the excitation is strongly delocalized over a dimer, and extends more weakly onto the neighboring BChls on either side. The results of Jimenez et al. [32] on fluorescence anisotropy can be understood if partial localization occurs during the preparation process (an instrument response of 160 fs), since the initial anisotropy is 0.4 rather than the larger value expected for a delocalized emitter [49, 72, 73]. It seems likely, therefore, that

localization precedes the 90–130 fs timescale ascribed to energy transfer in the 3PEPS data [53]. Given the strong localizing influences of disorder and nuclear motions, we estimate that localization occurs in, at most, 60 fs.

4. Conclusion

Purple bacteria utilize a sophisticated combination of pigments, pigment–pigment interactions and protein–pigment interactions to achieve an antenna system that is spatially large (compared to the RC) and spectrally broad. Despite the large number of antenna pigments present in the antenna, excitation energy is transferred to the RC with near unit efficiency. In this paper, we have described the recent work in our group to understand this energy transfer process.

We have used the TDC method, which gives accurate Coulombic couplings at all pigment separations, to estimate the coupling strengths between the pigments of LH2. These calculations show that carotenoid S_2–BChl Q_x energy transfer is rapid enough to be the dominant carotenoid–BChl pathway in LH2. Fluorescence upconversion experiments confirm this picture, showing more rapid decay of the carotenoid S_2 population *in vivo* than in solution and a concomitant rise in excited BChl population *in vivo*. Large *ab initio* calculations on an aggregate of two B850 BChl, a carotenoid and one B800 BChl show that electron density is shared between the B850 and the carotenoid, and that the presence of the carotenoid modifies the transition density of the B850. These changes in the B850 transition density suggest that the carotenoid may mediate the B800–B850 energy transfer.

Proper description of the B850 ring of LH2 and the B875 ring of LH1 requires a model including complex interplay between different factors which tend to delocalize (electronic coupling) or localize (static disorder and nuclear motions) excitation. We have used both electronic structure calculations and ultrafast spectroscopy to analyze these factors.

Electronic structure calculations, which estimate both the short-range (orbital overlap-dependent) and Coulombic (via the TDC method) contributions to the electronic coupling, estimate the intrapolypeptide coupling to be 315 cm^{-1} and the interpolypeptide coupling to be 245 cm^{-1}. These couplings are primarily determined by the Coulombic interaction, while the short-range term represents a small but significant $\sim 20\%$ of the total. Calculations which include the interaction of some protein residues with the BChls quantitatively reproduce the red shift shown to be induced by the presence of H-bonding residues, as well as increasing the intra- and interpolypeptide couplings to 335 cm^{-1} and 295 cm^{-1}, respectively. The presence of these residues also serves to partially reduce the difference in the α and β B850 transition energies brought about by their slightly different shape.

Photon echo measurements on LH1 and the B820 subunit can both be accurately simulated with identical parameters except for an energy transfer timescale, which is 90 fs in LH1 and ∞ in B820 (and 130 fs in LH2). The finding that the pair of BChl in B820 represents the entire LH1 ring well strongly suggests that disorder and dynamical processes localize the excitation. The weak temperature dependence of the peak shift of the B800–B820 (LH2) complex suggests that the dominant localizing effect is static disorder. Comparison of the strengths of localizing and delocalizing effects in the B850 and B875 rings leads us to believe

that excitation is localized on two to four pigments prior to the 90–130 fs energy transfer.

Despite the abundance of recent work, by many groups, related to the primary energy transfer process in photosynthetic purple bacteria, many questions remain. What are the short-range components of the carotenoid–BChl coupling? That is the role of the carotenoid S_1 state in energy transfer? How is rapid B800–B850 transfer realized? What is the precise nature of the initially prepared state in B850 and B875, and on what timescales does it evolve? Finally, our results point to a picture in which the protein plays a role in modifying electronic states and cannot be considered to be an inert scaffold only capable of influence by electrostatic energy shifts.

Acknowledgments

References

[1] G.R. Fleming, R. van Grondelle, *Physics Today* **47**, 48 (1994).

[2] R.K. Clayton, *Photosynthesis: Physical Mechanisms and Chemical Patterns*, Cambridge University Press, New York 1980.

[3] R. van Grondelle, J.P. Dekker, T. Gillbro, V. Sundström, *Biochim. Biophys. Acta* **1187**, 1 (1994).

[4] G. McDermott, S.M. Prince, A.A. Freer, A.M. Hawthornthwaite-Lawless, M.Z. Papiz, R.J. Cogdell, N.W. Isaacs, *Nature* **374**, 517 (1995).

[5] J. Koepke, X. Hu, C. Muenke, K. Schulten, H. Michel, *Structure* **4**, 581 (1996).

[6] S. Karrasch, P.A. Bullough, R. Ghosh, *EMBO J.* **14**, 631 (1995).

[7] X. Hu, A. Damjanovic, T. Ritz, K. Schulten, *Proc. Natl. Acad. Sci. USA* **95**, 5935 (1998).

[8] G.J.S. Fowler, R.W. Visschers, G.G. Grief, R. van Grondelle, *Nature* **355**, 848 (1992).

[9] A. Freer, S. Prince, K. Sauer, M. Papiz, A. Hawthornthwaite-Lawless, G. McDermott, R. Cogdell, N. Isaacs, *Structure* **4**, 449 (1996).

[10] S.M. Prince, M.Z. Papiz, A.A. Freer, G. McDermott, A.M. Hawthornthwaite-Lawless, R.J. Cogdell, N.W. Isaacs, *J. Mol. Biol.* **268**, 412 (1997).

[11] H.A. Frank, R.J. Cogdell, *Photochem. Photobiol.* **63**, 257 (1996).

[12] Y. Koyama, M. Kuki, P.O. Andersson, T. Gillbro, *Photochem. Photobiol.* **63**, 243 (1996).

[13] A.W. Rutherford, *Trends Biochem. Sci.* **14**, 227 (1989).

[14] D.R. Klug, J.R. Durrant, J. Barber, *Philos. Trans. R. Soc. Lond. A* **356**, 449 (1998).

[15] D.J. Kyle, I. Ohad, C.J. Arntzen, *Proc. Natl. Acad. Sci. USA* **81**, 4070 (1984).

[16] A.K. Mattoo, J.B. Marder, M. Edelman, *Cell* **56**, 241 (1989).

[17] J. Barber, B. Andersson, *Trends Biochem. Sci.* **17**, 61 (1992).

[18] R.J. Cogdell, H.A. Frank, *Biochim. Biophys. Acta* **895**, 63 (1987).

[19] B.P. Krueger, G.D. Scholes, G.R. Fleming, *J. Phys. Chem. B* **102**, 5378 (1998).

[20] B.P. Krueger, G.D. Scholes, R. Jimenez, G.R. Fleming, *J. Phys. Chem. B* **102**, 2284 (1998).

[21] T. Förster, in: *Modern Quantum Chemistry*, Ed. O. Sinanoglu, Vol. III, Academic Press, Inc., New York 1965, p. 93.

[22] F. London, *J. Phys. Chem.* **46**, 305 (1942).

[23] E.F. Haugh, J.O. Hirschfelder, *J. Chem. Phys.* **23**, 1778 (1955).

[24] K.D. Philipson, S.C. Tsai, K. Sauer, *J. Phys. Chem.* **75**, 1440 (1971).

[25] A. Golebiewski, A. Witkowski, *Rocz. Chem.* **33**, 1443 (1959).

[26] J.C. Chang, *J. Chem. Phys.* **67**, 3901 (1977).

[27] K. Sauer, R.J. Cogdell, S.M. Prince, A. Freer, N.W. Isaacs, H. Scheer, *Photochem. Photobiol.* **64**, 564 (1996).

[28] W.J. Hehre, L. Radom, P. v. R. Schleyer, J.A. Pople, *Ab Initio Molecular Orbital Theory*, John Wiley and Sons, New York 1986.

[29] P.O. Andersson, R.J. Cogdell, T. Gillbro, *Chem. Phys.* **210**, 195 (1996).

[30] M. Ricci, S.E. Bradforth, R. Jimenez, G.R. Fleming, *Chem. Phys. Lett.* **259**, 381 (1996).

[31] S. Mukamel, V. Rupasov, *Chem. Phys. Lett.* **242**, 17 (1995).

[32] R. Jimenez, S.N. Dikshit, S.E. Bradforth, G.R. Fleming, *J. Phys. Chem.* **100**, 6825 (1996).

[33] T. Pullerits, S. Hess, J.L. Herek, V. Sundström, *J. Phys. Chem. B* **101**, 10560 (1997).

[34] A.P. Shreve, J.K. Trautman, H.A. Frank, T.G. Owens, A.C. Albrecht, *Biochim. Biophys. Acta* **1058**, 280 (1991).

[35] G.D. Scholes, B.P. Krueger, I.R. Gould, G.R. Fleming, manuscript in preparation.

[36] G.R. Fleming, R. van Grondelle, *Curr. Opin. Struct. Biol.* **7**, 738 (1997).

[37] T. Pullerits, M. Chachisvillis, V. Sundström, *J. Phys. Chem.* **100**, 10787 (1996).

[38] J.-Y. Yu, Y. Nagasawa, R. van Grondelle, G.R. Fleming, *Chem. Phys. Lett.* **280**, 404 (1997).

[39] S.E. Bradforth, R. Jimenez, F. van Mourik, R. van Grondelle, G.R. Fleming, *J. Phys. Chem.* **99**, 16179 (1995).

[40] R. Monshouwer, M. Abrahamsson, F. van Mourik, R. van Grondelle, *J. Phys. Chem. B* **101**, 7241 (1997).

[41] H.M. Visser, F.J. Kleima, I.H.M. van Stokkum, R. van Grondelle, H. van Amerongen, *Chem. Phys. Lett.* **210**, 297 (1996).

[42] M. Chachisvilis, O. Kühn, T. Pullerits, V. Sundström, *J. Phys. Chem. B* **101**, 7275 (1997).

[43] M. Chachisvilis, T. Pullerits, M.R. Jones, C.N. Hunter, V. Sundström, *Chem. Phys. Lett.* **224**, 345 (1994).

[44] X. Hu, T. Ritz, A. Damjanovic, K. Schulten, *J. Phys. Chem. B* **101**, 3854 (1997).

[45] R.G. Alden, E. Johnson, V. Nagarajan, W.W. Parson, C.J. Law, R.G. Cogdell, *J. Phys. Chem. B* **101**, 4667 (1997).

[46] W.M. Zhang, T. Meier, V. Chernyak, S. Mukamel, *Philos. Trans. R. Soc. Lond. A* **356**, 405 (1998).

[47] Y. Nagasawa, J.-Y. Yu, M. Cho, G.R. Fleming, *Faraday Discuss. Chem. Soc.* **108**, 23 (1997).

[48] Y. Nagasawa, S.A. Passino, T. Joo, G.R. Fleming, *J. Chem. Phys.* **106**, 4840 (1997).

[49] R. Kumble, R.M. Hochstrasser, *J. Chem. Phys.* **109**, 855 (1998).

[50] M. Cho, G.R. Fleming, *Adv. Chem. Phys.* **107**, 312 (1998).

[51] M. Cho, J.-Y. Yu, Y. Nagasawa, S.A. Passino, G.R. Fleming, *J. Phys. Chem.* **100**, 11944 (1996).

[52] G.R. Fleming, T. Joo, M. Cho, *Adv. Chem. Phys.* **101**, 141 (1997).

[53] R. Jimenez, F. van Mourik, J.Y. Yu, G.R. Fleming, *J. Phys. Chem. B* **101**, 7350 (1997).

[54] S. Savikhin, W.S. Struve, *Chem. Phys.* **210**, 91 (1996).

[55] V. Nagarajan, R.G. Alden, J.C. Williams, W.W. Parson, *Proc. Natl. Acad. Sci. USA* **93**, 13774 (1996).

[56] T. Pullerits, V. Sundström, *Acc. Chem. Res.* **29**, 381 (1996).

[57] P.A. Loach, P.S. Parkes-Loach, in: *Anoxygenic Photosynthetic Bacteria*, Eds. R.E. Blankenship, M.T. Madigan, C.D. Bauer, Kluwer Academic Publishers, Dordrecht 1995, p. 437.

[58] J.T.M. Kennis, A.M. Streltsov, H. Permentier, T.J. Aartsma, J. Amesz, *J. Phys. Chem. B* **101**, 8369 (1997).

[59] O. Kühn, V. Sundström, *J. Chem. Phys.* **107**, 4154 (1997).

[60] McKluskey, S.M. Prince, N.W. Isaacs, R.J. Cogdell, unpublished results.

[61] G.D. Scholes, I.R. Gould, R.J. Cogdell, G.R. Fleming, submitted *J. Phys. Chem. B*.

[62] S. Hess, E. Åkesson, R.J. Cogdell, T. Pullerits, V. Sundström, *Biophys. J.* **69**, 2211 (1995).

[63] H.M. Visser, O.J.G. Somsen, F. van Mourik, S. Lin, I. van Stokkum, R. van Grondelle, *Biophys. J.* **69**, 1083 (1995).

[64] H. Zuber, *Photochem. Photobiol.* **42**, 821 (1985).

[65] R.A. Bunisholz, H. Zuber, *J. Photochem. Photobiol. B* **15**, 113 (1992).

[66] P.S. Parkes-Loach, J.R. Sprinkle, P.A. Loach, *Biochemistry* **27**, 2718 (1988).

[67] K.A. Meadows, P.S. Parkes-Loach, J.W. Kehoe, P.A. Loach, *Biochemistry* **37**, 3411 (1998).

[68] J.W. Kehoe, K.A. Meadows, P.S. Parkes-Loach, P.A. Loach, *Biochemistry* **37**, 3418 (1998).

[69] F.C. Spano, S. Mukamel, *J. Chem. Phys.* **91**, 683 (1989).

[70] W.M. Zhang, T. Meier, V. Chernyak, S. Mukamel, *J. Chem. Phys.* **108**, 7763 (1998).

[71] S. Hess, F. Feldchtein, A. Rabin, I. Nurgaleev, T. Pullerits, A. Sergeev, V. Sundström, *Chem. Phys. Lett.* **216**, 247 (1993).

[72] C.K. Law, R.S. Knox, J.H. Eberly, *Chem. Phys. Lett.* **258**, 352 (1996).

[73] A. Matro, J.A. Cina, *J. Phys. Chem.* **99**, 2568 (1995).